Draft version July 20, 2012
Preprint typeset using LaTeX style emulateapj v. 5/2/11

arXiv:1207.4541v1 [astro-ph.CO] 19 Jul 2012

FOUR NEW OBSERVATIONAL $H(Z)$ DATA FROM LUMINOUS RED GALAXIES SLOAN DIGITAL SKY SURVEY DATA RELEASE SEVEN

Cong Zhang[1], Han Zhang[1], Shuo Yuan [1], Tong-Jie Zhang [1,2] and Yan-Chun Sun[1]

Draft version July 20, 2012

ABSTRACT

By adopting the differential age method, we utilize selected 17832 luminous red galaxies (LRGs) from Sloan Digital Sky Survey Data Release Seven (SDSS DR7) covering redshift 0-0.4 based on 'Carson & Nichol sample' to measure Hubble parameters. With single stellar population (SSP) models, we derive optimal age information of our selected sample. From the decreasing age-redshift relation, we obtain the new observational $H(z)$ data (OHD) points which are $H(z) = 69.0 \pm 19.6$ km s^{-1} Mpc^{-1} at $z = 0.07$, $H(z) = 68.6 \pm 26.2$ km s^{-1} Mpc^{-1} at $z = 0.12$, $H(z)$=72.9 ± 29.6 km s^{-1} Mpc^{-1} at $z = 0.2$ and $H(z)$=88.8 ± 36.6 km s^{-1} Mpc^{-1} at $z = 0.28$, respectively. Combined with other 21 available OHD data points, a good performance of constraint on ΛCDM model is presented.

Subject headings: Cosmology:cosmological parameters -Cosmology: observations -Galaxies: evolution

1. INTRODUCTION

The expansion of the Universe can be quantitatively studied using the results from a variety of cosmological observations, for example the mapping of the cosmic microwave background (CMB) anisotropies (Spergel et al. 2007; Komatsu et al. 2010), the measurement of baryon acoustic oscillation (BAO) peaks (Eisenstein et al. 2005; Percival et al. 2010), the linear growth of large-scale structures (LSS) (Wang & Tegmark 2004), strong gravitational lensing (Yang & Chen 2009; Cao et al. 2012), and measurements of 'standard candles' such as the redshift-distance relationship of type Ia supernovae (SNIa) (Riess et al. 1998; Li et al. 2011) and gamma-ray bursts (GRBs)(Ghirlanda et al. 2004; Li et al. 2008). Among the various observations is the determination of the Hubble parameter $H(z)$ which is directly related to the expansion history of the Universe by its definition: $H(z) = \dot{a}/a$, where a denotes the cosmic scale factor and $\dot{a}$ is its rate of change with respect to the cosmic time. The method based on the observational $H(z)$ data (OHD) has been used to test cosmological models (e.g., Yi & Zhang 2007; Samushia & Ratra 2006; Zhang et al. 2007; Zhang & Zhu 2008; Carvalho et al. 2008; Feng & li 2010; Chen & Ratra 2011; Xu 2012). Besides parameters constraints, OHD can also be used as an auxiliary model selection criterion (Li et al. 2009).

In practice, the Hubble parameter $H(z)$ is usually measured as a function of the redshift z, with $a(t)/a(t_0) = 1/(1 + z)$:

$$H(z) = -\frac{1}{1+z}\frac{dz}{dt}. \qquad (1)$$

According to equation (1), $H(z)$ has been measured through the differential method, which was first put forward by Jimenez & Loeb (2002). Derivative of redshift with respect to cosmic time, dz/dt has a direct determination on $H(z)$. This method has been demonstrated in Jimenez et al. (2003) and Simon et al. (2005) who extended the determination of $H(z)$ to 8 more redshift bins up to $z \approx 1.8$. This dataset was brought up-to-date by Stern et al. (2010).

However, it may be difficult to determine the accurate age of a galaxy considering stars in a galaxy born continuously, and a young stellar population may dominate their emission spectra (Zhang et al. 2010). Fortunately, it has been found in great number that luminous red galaxies (LRGs) which have photometric properties consistent with an old, passively evolving stellar population (Roseboom et al. 2006) could be selected as 'cosmic chronometers' (Crawford et al. 2010).

Different from other methods of obtaining the age history of galaxies by co-adding spectra (e.g., Carson & Nichol 2010), we employ ULySS, an available package on-line to fit a full-length spectrum. Through single stellar population (SSP) fitting, age information could be obtained which will be discussed in detail in Section 3. From the age-redshift relation, OHD points could be deduced finally.

There are already 21 OHD points obtained from both differential age method and baryon acoustic oscillation (BAO) method (Moresco et al. 2012; Stern et al. 2010; Simon et al. 2005; Gaztañaga et al. 2009). Currently the number of OHD points are still scarce compared with SNIa luminosity distance data. Therefore the potential power of OHD in constraining cosmological parameter is explored in Ma et al. (2011) in detail. It has been found that as many as 64 further independent determination of $H(z)$ are needed to match the parameter constraining power of SN Ia. In Section 5, we combine our 4 new data points with those 21 OHD points to constrain cosmological parameter.

This paper is organized as follows. We briefly give our LRGs selection sample in Section 2. In Section 3, we describe explicitly how we gain the age information from the LRG spectra using ULySS and in Section 4 we present our method to get the OHD using the galaxy ages. A cosmology constraint using all available OHD including our 4 new ones is given in Section 5. Finally, in last section, we discuss the limitation and implication of our results.

---

[1] Department of Astronomy, Beijing Normal University, Beijing 100875, P.R.China;
[2] Center for High Energy Physics, Peking University, Beijing 100871, P. R. China; tjzhang@bnu.edu.cn

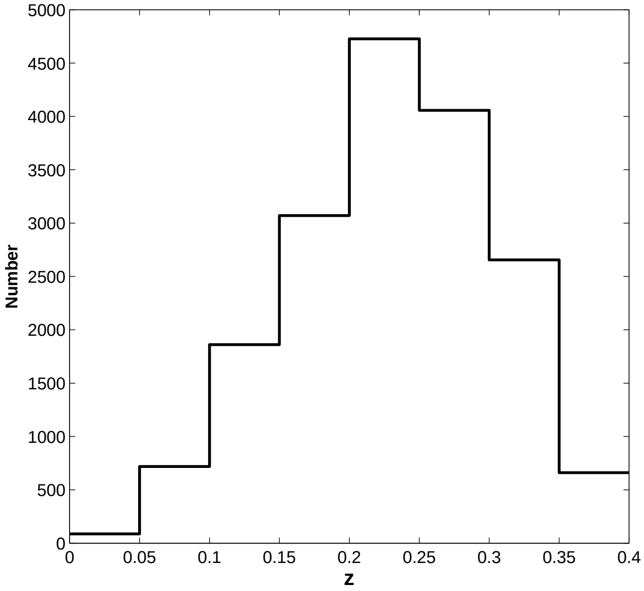

Figure 1. Redshift distribution of 17832 LRGs.

2. SOURCE SELECTION OF LRG SAMPLE

SDSS DR7 (Abazajian et al. 2009) includes 11,663 deg^2 of imaging data, with most of the 2000 deg^2 increment over the previous data release lying in regions of low Galactic latitude. The catalog contains five-band photometry for 357 million distinct objects. The survey also includes repeat photometry on a 120° long, 2.5° wide stripe along the celestial equator in the Southern Galactic Cap, with some regions covered by as many as 90 individual imaging runs.

The LRG selection criterions of SDSS Eisenstein et al. (2001) are on the basis of color and magnitude to yield a sample of luminous, intrinsically red galaxies. However, the sample selected from SDSS according to Eisenstein's selection criterion are not very homogeneous. Our sample has been extracted from Carson & Nichol's sample (Carson & Nichol sample; Carson & Nichol 2010) with a further restraint on signal to noise ratio (SNR). As SNR has an impact on our next fitting step, it is necessary to demand SNR of R-band to be greater than 10. The 17832 selected quiescent, luminous red galaxies basing on 'Carson & Nichol sample' method from SDSS DR7 cover the redshift range from 0-0.4, and the distribution of all LRGs is shown in Figure 1.

Compared with other spectra selection work, 'Carson & Nichol sample' calibrates, for the first time, the SDSS spectra on Lick/Image Dissector Scanner (IDS) system (Burtein et al. 1984; Worthey et al. 1994). Their general selected criterion steps are as followings. First step is to get LRGs from Catalog Archive Server (CAS) as outlined in Eisenstein et al. (2001). Further, restraining the spectrum using standard emission lines such as Hα, Hβ and OIII 5007 to increase the number of truly quiescent galaxies in the previous sample. To fully picture physical properties such as velocity dispersion and absolute luminosity of these LRGs, through correcting velocity dispersions for aperture effects and performing $K + e$ corrections to the magnitude, four subsamples are produced with different absolute magnitude and velocity dispersion. For a explicit description of this method, please refer to Carson & Nichol (2010).

3. AGE-REDSHIFT RELATION

We proceed to describe our way of obtaining age information of LRGs. In this paper we employ ULySS (Koleva et al. 2009a) to analyze the selected spectra. This package is available at http://ulyss.univ-lyon1.fr/. In ULySS, an observed spectrum is fitted with a model expressed as a linear combination of non-linear components (Koleva et al. 2009a). The full spectrum is utilized in fittings for determination of the star formation and metal enrichment history of galaxies (Wu et al. 2011a). This package minimizes χ^2 between an observed spectrum and a model spectrum. This method has already been successfully tested in Wu et al. (2011b). The reliability and robustness of using ULySS to the study of the history of stellar population has been verified (e.g., Koleva et al. 2009b; Koleva et al. 2009c; Bouchard et al. 2010; Makarova et al. 2010).

3.1. *Matching resolution*

The first step in fitting is to match resolutions between the observed spectra and the model we use. To match the resolution of our LRG spectra from SDSS DR7 to the models, we transform the model provided by ULySS by injecting relative line spread function (LSF) between our spectrum and the model. When determining the LSF, we make use of the available velocity dispersion template stars as a standard star from http://www.sdss.org/dr7/algorithms/veldisp.html. We make a five times linear interpolation in wavelength and convolve with the model. In this way, a new matching model is generated, and all this process could be accomplished through ULySS function (Koleva et al. 2009a).

3.2. *Single stellar population result*

It is essential to study the stellar population of galaxies if we want to reconstruct the star formation history (SFH) of galaxies. We fit the spectrum with a single SSP for the following reasons. Firstly, LRG is believed to be drawn from a same parent population with the most percent of their stars are formed from a single-burst. Secondly, SSP-equivalent properties correspond to the 'luminosity-weighted' average over the distributions. Thus by a single SSP fitting, a general view of a galaxy could be gotten (Du et al 2010). We carry out an initial study of age-dating using the stellar population models of Bruzual & Charlot (2003) (BC03) to synthesize spectra, and this model is also provided by ULySS.

BC03 is a model for computing the spectral evolution of stellar populations at ages between 1×10^5 yr and 2×10^{10} yr at a resolution of 3 $\mathring{A}$ across the whole wavelength range from 3200 $\mathring{A}$ to 9500 $\mathring{A}$ for a wide range of metallicities (Bruzual & Charlot 2003). The accuracy of this model has been proved and it has been widely used for getting information of spectra. But when interpreting the galaxy spectra, we find both of age and metallicity guess value tend to affect the fitting result. It is difficult to remove such influence especially at the low resolving spectra (Du et al 2010). The fitting of ULySS starts from a point (initial value) in the parameter space(age

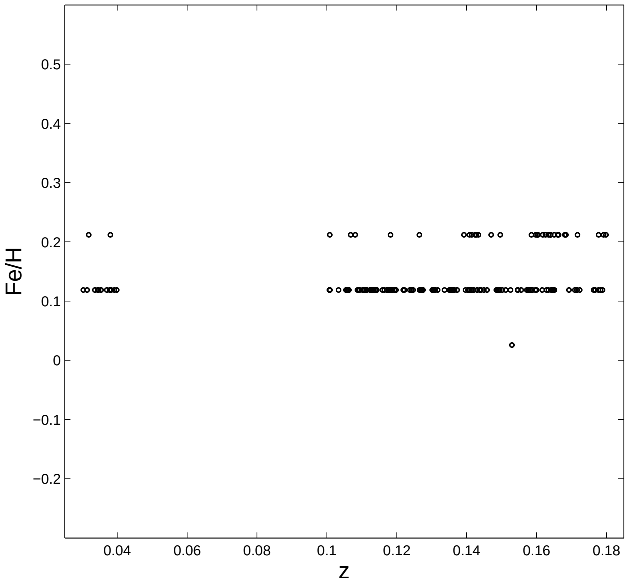

Figure 2. Redshift-metallicity relationship from χ^2 map (40×40). Open circles correspond to a subsample of 164 LRGs. It shows that all galaxies metallicity are consistent and fluctuate between 0.1 to 0.2 dex approximately.

and metallicity), therefore we stress the importance of that point as the returning fitting value will be initial value dependent and the minimization will be local. In order to identify and understand the age-metallicity degeneracy and local minimizations, we analyze that age-metallicity degeneracy and construct χ^2 map which is a function provided by ULySS. The χ^2 map is a visualization of parameters space, and the principle of this map is to give a grid of nodes in a 2-D projection of the parameter space. χ^2 map returns the minimization of each node (Koleva et al. 2009a).

A subsample of 164 LRG spectra from redshift 0.03 to 0.179 is dealt with by building their χ^2 maps. The metallicity results of this sample are shown in Figure 2. From Figure 2, it has been discovered that the metallicity of LRGs are consistent with the assumption that selected galaxies are thought to be have similar metallicities (Jimenez et al. 2003) and it floats between about 0.1 dex and 0.2 dex (see Figure 2).

ULySS could provide initial value vectors as initial value, that is to say, if giving points intensive enough, it is possible to find the global minimization and thus break the degeneracy. We set our metallicity range guess points from 0.1-0.2 dex to every galaxy in our sample, while age guess point span from 5000 Myr-11200 Myr.

For each galaxy, groups of age and metallicity values can be gained as results. We ignore the metallicity and just focus on the age. To identify the final accurate age of each galaxy, we base our selections on the minimal χ^2 criterion. In particular, if all fitting ages for a single galaxy surpass the age of our universe, it is not convincing as there are several reasons causing this situation such as the low resolution of spectra and model dependence. After removing the result whose $a_i + \sigma_i$ is greater than 16 Gyr, where a_i is the age and σ_i is the age error, LRG ages are obtained and the age distribution is displayed in Figure 3. Figure 4 shows the ages of galaxies as a function of redshift. For clarity, the ages less than 7 Gyr have not been plotted.

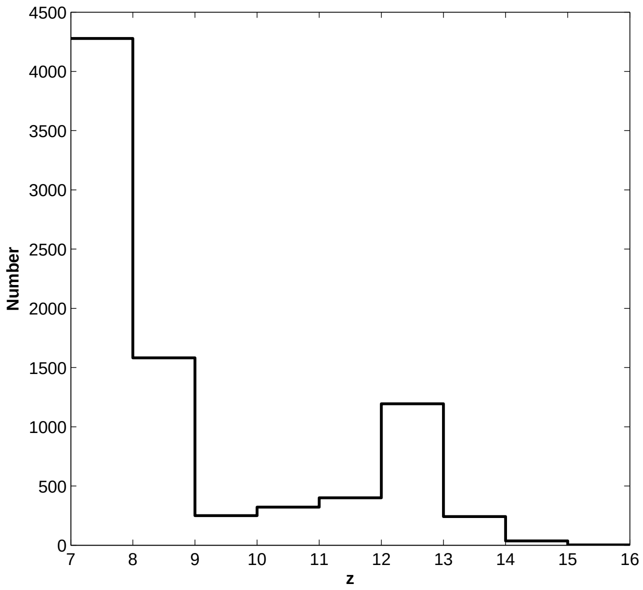

Figure 3. Histogram of age spread information. This diagram shows the age result of 17832 LRGs with age interval of 1.0 Gyr.

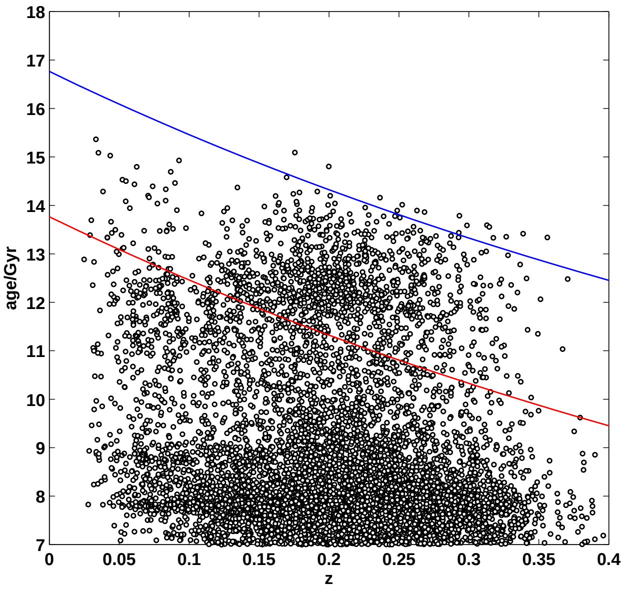

Figure 4. Age-redshift envelope obtained from the galaxies studied in this paper. Open circles correspond to LRGs from SDSS DR7. The red line shows the age of the universe $t(z)$ for a ΛCDM model with $\Omega_m = 0.29$ and $H_0 = 69$ km s^{-1} Mpc^{-1} while the blue line indicates $t(z) + 3Gyr$ and is for reference only. A clear trend is present: galaxies age as redshift decreases.

4. THE DETERMINATION OF OHD

By using the age-redshift relation for SDSS LRGs, we now determine the Hubble parameter $H(z)$. This procedure relies upon pinning down the 'edge' of the galaxy

Table 1
Result of fitting

	The result of the first sample					The result of the second sample				
n	4	5	6	7	8	5	6	7	8	9
$P_{\geq\chi^2}$	0.90012	0.94452	0.99009	0.98043	0.99315	0.96903	0.91520	0.99726	0.99203	0.97960
SSE/n	0.0526	0.0758	0.0492	0.1064	0.0947	0.2506	0.9640	0.3193	0.8018	1.5750
$slope$[a]	-9.53	-12.54	-13.23	-15.77	-15.50	-13.42	-6.61	-12.69	-12.46	-11.08
σ_{slop}	6.07	5.49	3.76	4.88	4.33	6.53	9.62	4.85	6.74	8.24
$-\sigma_{slop}/slope$	0.64	0.44	0.28	0.31	0.28	0.49	1.45	0.38	0.54	0.74
H[b]	96.5	72.8	69.0[c]	57.9	58.9	64.8	131.5	68.6[c]	69.9	78.8
	The result of the third sample					The result of the forth sample				
n	4	5	6	7	8	10	11	12	13	14
$P_{\geq\chi^2}$	0.94508	0.99194	0.99876	0.99867	0.99971	1.00000	1.00000	1.00000	1.00000	1.00000
SSE/n	0.0282	0.0198	0.0169	0.0338	0.0309	0.20844	0.1130	0.1752	0.1631	0.2109
$slope$[a]	-11.40	-14.44	-11.14	-11.83	-12.12	-11.70	-7.20	-8.61	-7.34	-7.81
σ_{slop}	12.33	6.19	4.53	5.86	5.34	4.75	3.09	3.55	3.15	3.38
$-\sigma_{slop}/slope$	1.08	0.43	0.41	0.50	0.44	0.41	0.43	0.41	0.43	0.43
H[b]	71.4	56.5	72.9[c]	68.7	67.0	65.4	106.3	88.8[c]	104.1	98.0

[a] $slope = dt/dz$, where t is the age of galaxies in the unit of Gyr.
[b] $H(z)$ is in units of km $\mathrm{s}^{-1}\mathrm{Mpc}^{-1}$.
[c] Four new OHD obtained in this paper.

age distribution in different redshift intervals.

The main trunk of our produce is to fit the data $t(z_i)$, which is the oldest age at redshift z_i with straight line and its slope dz/dt is related to the Hubble parameter at an effective redshift by $H(z_{eff} = -[1/(1+z_{eff})](dt/dz)^{-1}$ where $z_{eff} = (z_{max} + z_{min})/2$.

Mathematically, $z_{max} - z_{min}$ should not be too great, so we divide these data points into four parts, each of which is called, expediently, a 'subsample' based on redshift which are $0.03 \leq z \leq 0.11$, $0.08 \leq z \leq 0.16$, $0.16 \leq z \leq 0.24$, and $0.24 \leq z \leq 0.32$. Then we fit each 'subsample' by dividing it into suitably large redshift bins and get four new OHD finally.

However, a problem is how to determine the number of bins, n. Practically, because of the incomplete LRGs sample, the age obtained is perhaps not the really oldest at that redshift point, that is to say, the age selected is perhaps the 'fake oldest'. We should try to avoid picking up 'fake oldest' age for the accuracy of our result, but too large n may increase the risk of picking up the 'fake oldest'. To indicate this risk, SSE/n (average of the Sum of Squares for Error), which is proportional to this risk, is calculated. Of course the number of 'n' should not yet be too small in order to limit the statistical error which is proportional to the value of $\sigma_{slope}/slope$. So we divide each 'subsample' into 3, 4, $\cdots$, 20 bins respectively,and every time we divide, we calculate the parameter $\mathbf{\Delta} = (SSE/n,\ \sigma_{slope}/slope,\ ^1P_{\geq\chi^2})$. Finally, we compare all the parameters of $\mathbf{\Delta}$ to get the value of 'n'. But, there is something more to say, in the third and forth 'subsample', the error of the age is so big that the $P_{\geq\chi^2}$ is not such a good parameter to represent the goodness of fit. So in these 'subsamples', we consider the other two parameters more than the $P_{\geq\chi^2}$ when we choose the result. Especially for the forth 'subsample', it is too large relative errors of slope that lead us to $n \geq 10$ (see in Table 1). In addition, the optimal fitting of each part is also plotted in Figure 5. Finally we get four new OHD totally, which are $H(z)$=69.0 ± 19.6 km $\mathrm{s}^{-1}\mathrm{Mpc}^{-1}$ at $z = 0.07$, $H(z)$=68.6 ± 26.2 km s^{-1} Mpc^{-1} at $z = 0.12$, $H(z)$=72.9 ± 29.6 km $\mathrm{s}^{-1}\mathrm{Mpc}^{-1}$ at $z = 0.2$ and $H(z)$=88.8 ± 36.6 km $\mathrm{s}^{-1}\mathrm{Mpc}^{-1}$ at $z = 0.28$. Table 2 summarizes all the available OHD including the four new ones, and displayed in Figure 6.

Table 2
$H(z)$ measurements and their errors

z	$H(z)$ (km s^{-1}Mpc)	$\sigma_{H(z)}$ (km s^{-1}Mpc)	Reference
0.090	69	12	1
0.170	83	8	1
0.270	77	14	1
0.400	95	17	1
0.900	117	23	1
1.300	168	17	1
1.430	177	18	1
1.530	140	14	1
1.750	202	40	1
0.480	97	62	2
0.880	90	40	2
0.179	75	4	3
0.199	75	5	3
0.352	83	14	3
0.593	104	13	3
0.680	92	8	3
0.781	105	12	3
0.875	125	17	3
1.037	154	20	3
0.24	79.69	3.32	4
0.43	86.45	3.27	4
0.07	69.0	19.6[a]	
0.12	68.6	26.2[a]	
0.20	72.9	29.6[a]	
0.28	88.8	36.6[a]	

References. — 1.Simon et al. (2005) 2.Stern et al. (2010) 3.Moresco et al. (2012) 4.Gaztañaga et al. (2009)
[a] New OHD points obtained in section 4.

5. COSMOLOGICAL CONSTRAINTS FROM OHD

According to the Einstein gravity and Friedmann-Robertson-Walker (FRW) metric, $H(z)$ read theoretically:

$$H(z) = H_0\sqrt{\Omega_m(1+z)^3 + \Omega_\Lambda + \Omega_k(1+z)^2}, \qquad (2)$$

---

[1] $P_{\geq\chi^2}$ is the probability of obtaining equal or greater value of the reduced χ^2 if the $t(z)$ points are truly lying on a straight line

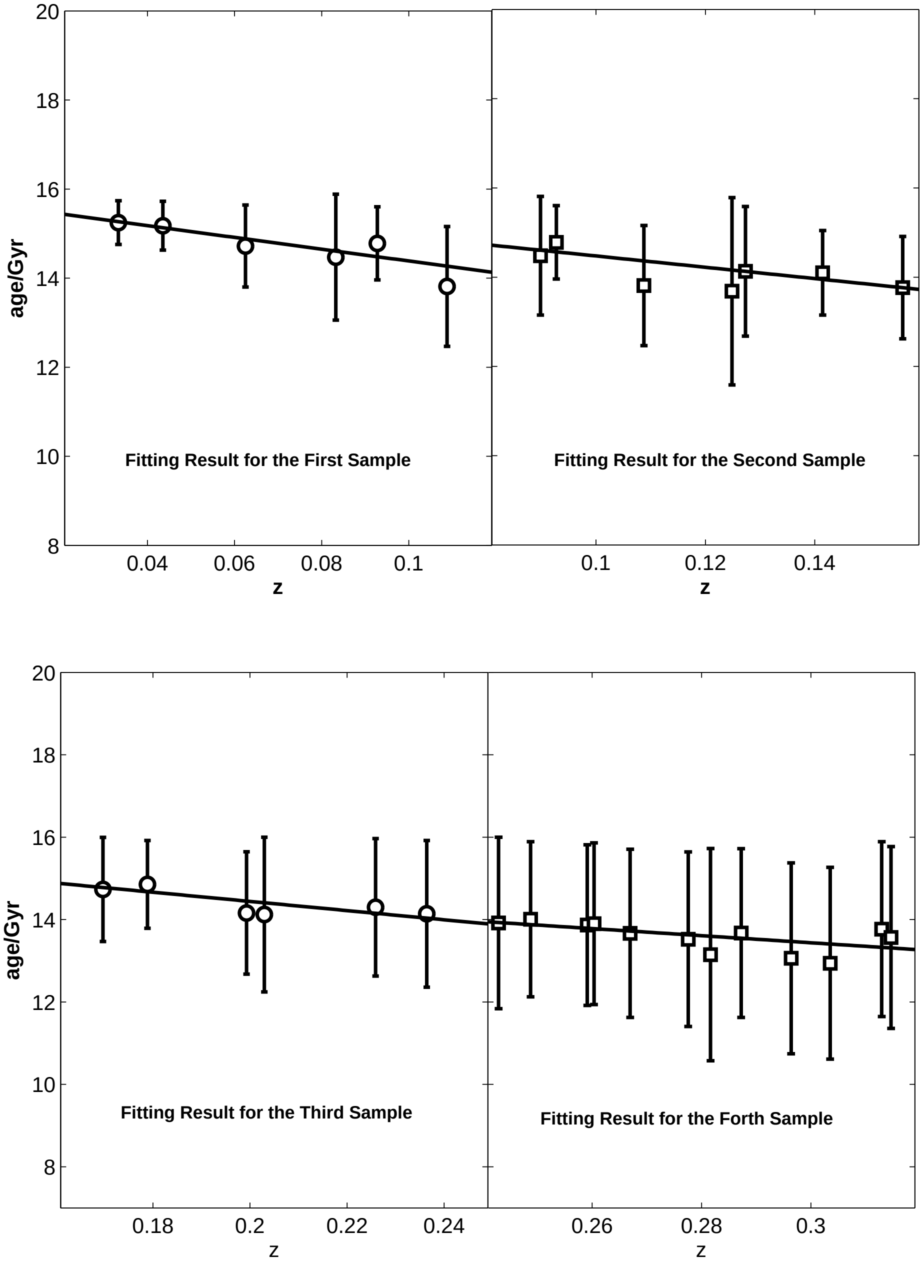

Figure 5. The optimal fitted results. The solid line represents the best fitting for each sample. In the first sample $z_{min} = 0.033$, $z_{max} = 0.109$, and $z_{eff} = 0.07$. In the second sample, $z_{min} = 0.090$, $z_{max} = 0.156$, $z_{eff} = 0.12$. In the third sample, $z_{min} = 0.170$, $z_{max} = 0.236$, $z_{eff} = 0.20$, and in the forth sample, $z_{min} = 0.243$, $z_{max} = 0.315$, $z_{eff} = 0.28$.

where Ω_r is ignored as it is too tinny at present ($\approx 4.183 \times 10^{-5}h^{-2}$), and $\Omega_m + \Omega_\Lambda + \Omega_k = 1$. Parameters Ω_m, Ω_Λ and Ω_k parameterize the density of matter, cosmological constant and curvature density. The best fit parameters of the model via OHD are determined by minimizing the χ^2:

$$\chi^2_{OHD}(\mathbf{p_{model}}) = \sum_{i=1}^{N} \frac{(H_{obs}(z_i) - H_{th}(z_i))^2}{\sigma^2_{obs,i}}, \qquad (3)$$

where $\mathbf{p_{model}}$ is a free parameter. Based on the basic equations of ΛCDM model, we have the following two models: for a flat ΛCDM($\Omega_k = 0$), $H_{th}(z) = H_0\sqrt{\Omega_m(1+z)^3 + (1-\Omega_m)}$ with $\mathbf{p_{flat}} = (\Omega_m, H_0)$; for a non-flat ΛCDM, $H_{th}(z) = H_0\sqrt{\Omega_m(1+z)^3 +) + \Omega_\Lambda + (1-\Omega_\Lambda-\Omega_m)(1+z)^2}$, with $\mathbf{p_{non-flat}} = (\Omega_\Lambda, \Omega_m, H_0)$. For both models, the likelihood function can be written as $L \propto$ exp $(-\chi^2_{OHD}/2)$.

We use MCMC method to calculate the likelihood in the independent parameter space. The Markov chains are generated and analyzed via the Python MCMC code – Pymc (Patil et al. 2010). The parameter H_0 and the density parameter $\mathbf{\Omega} = (\Omega_m,\ \Omega_\Lambda)$ are treated as independent parameters in these two models (Wei 2010), and all of the prior distributions of them are set as the uniform

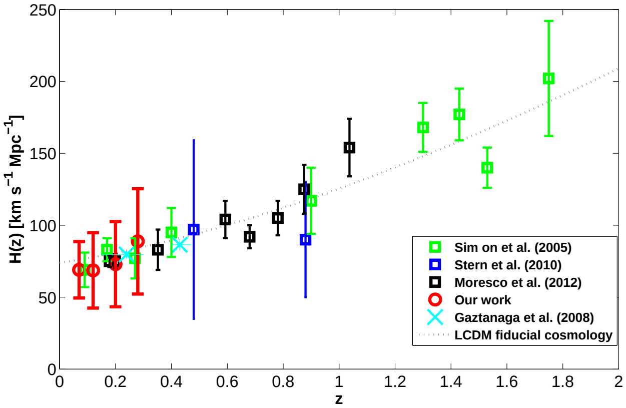

Figure 6. All available OHD points. The dashed line plots the theoretical Hubble parameter H_{fid} as a function of z from the spatially flat ΛCDM model with $\Omega_m = 0.3$, $\Omega_\Lambda = 0.7$, and $H_0 = 72$ km s^{-1}Mpc^{-1}.

Table 3
The Prior of Model Parameters

Model Parameters	Prior Distrubution
Ω_m	Uniform(0.0,1.5)[a]
Ω_Λ	Uniform(0.0,2.5)[a]
H_0	Uniform(50,100)[a]

[a] *Uniform(lower limit,upper limit)* stand for an uniform distribution in the interval [lower limit,upper limit], and the same below.

distribution (Table 3).

Figure 7 and Figure 8 show the one-dimensional marginalized probability distribution for each parameter at the diagonal positions and the two-dimensional marginalized confidence regions at the non-diagonal positions of the flat ΛCDM model and non-flat ΛCDM model respectively. The 3σ-s confidence regions (68.7%, 95.45%, 99.73%) for each parameter are calculated detailedly. The best fit parameters are pointed out in the contour plots with a long vertical line and a long horizonal line across.

To compare the constraining results of the 'new version OHD' within the new points we obtained and the 'old version OHD', Figure 7 and Figure 8 show both two results of the same model with different line colors to distinguish: the red lines referring to the 'new version OHD' and the blue ones means the 'old version OHD'.

The constraints in Figure 7 and Figure 8 show the well performances on constraining ΛCDM. On the flat-ΛCDM case, what we obtain of 'old version OHD' and 'new version OHD' are shown in Table 4 and for a non-flat scenario, the constraints are shown in Table 5. The new added-in points make amendments to the 'old version OHD'. In Fig 7 and Fig 8 the 1-D marginalized constraints are more stringent than the old one and for the same model the contour plots against the same parameters pair have more shrunk confidence region at the same level. Since the number of new added-on points is so small, the degree of shrinking is weak as well.

6. CONCLUSION AND DISCUSSION

In this paper we present our measurement of four new OHD points from the ages of passively-evolving galaxies at $z < 0.4$. A large sample of LRGs spectra has been dated by us and a age-redshift relation is obtained and displayed. By computing the relative ages of these LRGs, we give the final results on OHD. Combining them with other available 21 OHD points, we constrain cosmological parameters using the update samples of OHD. The new added-in points data make amendments to the 'old version OHD'. The 1-D marginalized constraints is more stringent than the old one and for the same model the contour plots against the same parameters pair have more shrunk confidence region at the same level. Since the number of new added-on points is so small, the degree of shrinking is weak as well.

As our selected LRGs are incomplete and unable to cover all old-age galaxies in the universe, there would bring some difficulty in tracing the 'cosmic chronometers', that is to say, oldest age in our sample may not represent cosmic age at that redshift. It would be improved through future redshift surveys of observation and lead to successful realization of differential age method. In addition, as high SNR is essential for a precise fitting which determines the age of galaxies, we suggest that the accuracy of OHD would be improved if the SNR of spectra would increase. We employ ULySS to reconstruct the stellar population of galaxies. Though the robustness of ULySS has been illustrated, the fitting minimal may still be local because of the limitation of groups of initial values. There has been significant advancement in modeling stellar populations of LRG galaxies and we expect these to improve the accuracy in this process in the future.

The number of OHD is still scarce currently compared with SNIa data sets. OHD plays almost the same role as that of SNIa for the joint constraints on the ΛCDM model. The number of OHD points would extended in further decades with more and deeper observation of galaxies and at that time OHD set lone is capable to be used in place of current SNIa data sets (Ma et al. 2011). Fortunately, we have seen that BOSS project and proposed Sandage-Loeb observational plan (Corasaniti et al. 2007) can be used to extend our knowledge of cosmic expansion into the even deeper redshift. Finally, we think it is reasonable to expect that OHD will complement SNIa, BAO and weak lensing and help us getting more knowledge of the evolution history of our universe.

ACKNOWLEDGMENTS. Special thanks to Robert C. Nichol and Dan P. Carson for providing us the LRG sample data. We are grateful to G. Bruzual, M. Koleva, Wei Du, Gao-Chao Liu, Xian-Bin Meng and C. Ma for their helpful so many suggestions. This work was supported by the National Science Foundation of China (Grants No. 10473002), the Ministry of Science and Technology National Basic Science program (project 973) under grant No. 2009CB24901, and the Fundamental Research Funds for the Central Universities.

REFERENCES

Abazajian, K. N. et al. 2009, ApJ, 726, 98
Bouchard, A., Prugniel, P., Koleva, M., Sharina, M. 2010, A&A, 513, 54

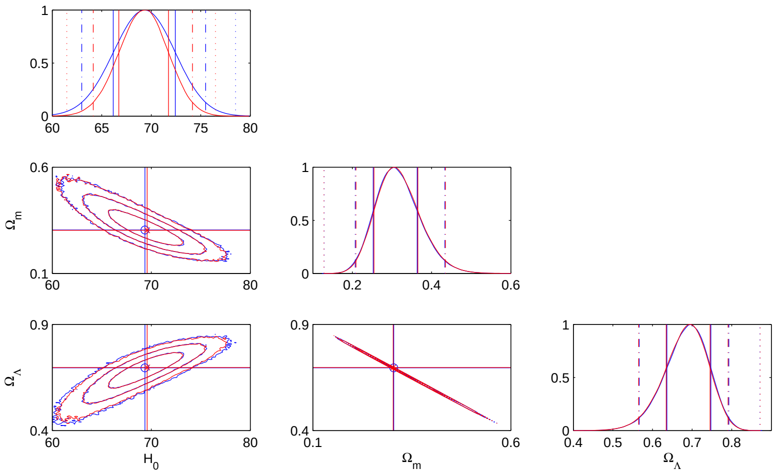

Figure 7. OHD Constraining results of flat ΛCDM. The diagonal plots show the 1-D PDF and the vertical lines from center to edge matches the 3σ-s intervals. The non-diagonal plots show the 2-D confidence regions with contours for inner to outer matches the 3σ-s levels, and the open blue circle point out the best fit point by 'old version OHD' while the red cross shows the ones via 'new version OHD'.

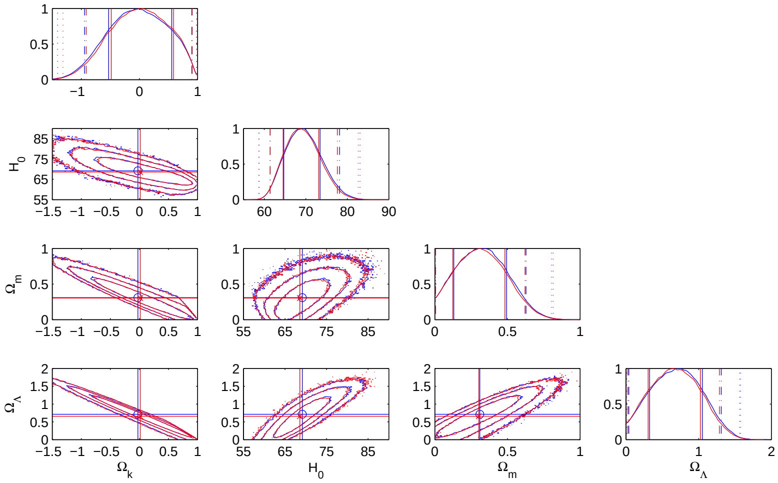

Figure 8. OHD Constraining result of non-flat ΛCDM. The diagonal plots show the 1-D PDF and the vertical lines from center to edge match the 3σ-s intervals. The non-diagonal plots show the 2-D confidence regions with contours for inner to outer match the 3σ-s levels, and the open blue circle point out the best fit point by 'old version OHD' while the red cross show the ones via 'new version OHD'.

Table 4

Marginalized Constraints on Ω_m, Ω_Λ and H_0 for **flat ΛCDM** Model

Model Parameters	Old Version OHD	New Version OHD
Ω_m[a]	$0.304354^{+0.059338\ +0.129278\ +0.378909}_{-0.051703\ -0.097228\ -0.175343}$	$0.302981^{+0.062313\ +0.132125\ +0.418484}_{-0.048496\ -0.093698\ -0.174888}$
Ω_Λ	$0.695646^{+0.051703\ +0.097228\ +0.175343}_{-0.059338\ -0.129278\ -0.378965}$	$0.697019^{+0.048496\ +0.093698\ +0.174826}_{-0.062313\ -0.132125\ -0.418484}$
$\mathrm{H_0}(\mathrm{km\ s^{-1}Mpc^{-1}})$	$69.358015^{+3.076828\ +6.134441\ +9.162546}_{-3.192755\ -6.377486\ -9.625775}$	$69.589234^{+2.154653\ +4.570973\ +6.899727}_{-2.860217\ -5.446933\ -8.114114}$

[a] The errors are 1σ error, 2σ error and 3σ error, similarly hereinafter

Table 5

Marginalized Constraints on $\Omega_m, \Omega_\Lambda, \Omega_k$ and H_0 for **non-flat** Λ**CDM** Model

Model Parameters	Old Version OHD	New Version OHD
Ω_k	$-0.026853^{+0.582170\ +0.927979\ +1.010927}_{-0.502165\ -0.917479\ -1.379130}$	$0.013140^{+0.572778\ +0.894003\ +0.968714}_{-0.499037\ -0.928112\ -1.326954}$
Ω_m	$0.310045^{+0.183918\ +0.317614\ +0.504268}_{-0.179401\ -0.304774\ -0.304774}$	$0.302706^{+0.180116\ +0.318419\ +0.499922}_{-0.179044\ -0.296992\ -0.296992}$
Ω_Λ	$0.711812^{+0.340111\ +0.599591\ +0.865635}_{-0.386973\ -0.672324\ -0.702056}$	$0.658208^{+0.366158\ +0.627745\ +0.904253}_{-0.354011\ -0.633352\ -0.648651}$
$\mathrm{H}_0(\mathrm{km\ s}^{-1}\mathrm{Mpc}^{-1})$	$69.181938^{+4.282564\ +8.981085\ +13.888657}_{-4.477042\ -7.739618\ -10.453862}$	$68.582621^{+4.559844\ +9.046496\ +14.061616}_{-4.026863\ -7.140919\ -9.811629}$

Bruzual, G., & Charlot, S. 2003, MNRAS, 344, 1000
Burtein, D., Faber, S. M., Gaskell, C. M., Krumm, N. 1984, ApJ, 287, 586
Carvalho, F. C., Santos, E. M., Alcaniz, J. S. and Santos, J. 2008, J. Cosmology Astropart.Phys, 09, 008
Carson, D. P., & Nichol, R. C. 2010, MNRAS, 408, 213
Cao S., Pan Y., Biesiada M., Godlowski W., Zhu Z. H. 2012, J. Cosmology Astropart.Phys, 03, 016
Chen, Y. & Ratra, B. 2011, Phys. Lett. B, 703, 406
Corasaniti, P., Huterer, D., & Melchiorri, A. 2007, Phys. Rev. D, 75, 062001,
Crawford, S. M., Ratimbazafy, A. L., Cress, C. M., et al. 2010, MNRAS, 406, 2569
Du, W., Luo, A. L., Prugniel, Ph., Liang, Y. C., & Zhao, Y. H. 2010, MNRAS, 409, 567
Eisenstein, D. J. et al. 2001, AJ, 122, 2267
Eisenstein, D. J. et al. 2003, ApJ, 585, 694
Eisenstein, D. J. et al. 2005, ApJ, 633, 560
Figueroa, D. G., Verde, L., Jimenez, R. 2008, J. Cosmology Astropart.Phys, 08, 038
Feng, C.-J. & Li, X.-Z. 2010, Phys. Lett. B, 692, 152
Gaztañaga, E., Cabré, A., Hui, L. 2009, MNRAS, 399, 1663
Ghirlanda, G., Ghisellini, G., Lazzati, D., & Firmani, C. 2004, ApJ, 613, L13
Jimenez, R., Verde, L., Treu, T., Stern, D. 2003, AJ, 593, 622
Jimenez, R., Loeb, A., 2002, ApJ, 573, 37
Jimenez, R., Talavera, P., Verde, L. 2011, J. Cosmology Astropart.Phys, arXiv:1107.2542v1
Komatsu, E. et al. 2010, ApJS, arXiv:1001.4538
Koleva, M., Prugniel, Ph., Bouchard, A., & WU., Y. 2009a, A&A, 501, 1269
Koleva, M., Prugniel, Ph. et al. 2009b, AN, 330, 960
Koleva, M. et al. 2009c, MNRAS, 396, 2133
Li, H., Xia, J.-Q., Liu, J., Zhao, G.-B., Fan, Z.-H., & Zhang, X. 2008, ApJ, 680, 92
Li, M., Li, X.-D., Wang, S., & Zhang, X. 2009, J. Cosmology Astropart.Phys, 06, 036
Li, Z. X., Wu, P. X., & Yu, H. W. 2011, Phys. Lett. B, 695, 01
Ma, C., Zhang, T.-J. 2011, ApJ, 730, 74
Makarova, L., Koleva, M., Makarov, D., Prugniel, Ph. 2010, MNRAS, 406, 1152
Moresco, M., Cimatti, A., Jimenez, R. et al. 2012, J. Cosmology Astropart.Phys, arXiv:1201.3609v1
Patil, A., Huard, D., Fonnesbeck, C. J. 2010, Journal of Statistical Software, 35(4), 1-81
Percival, W. J. et al. 2010, MNRAS, 401, 2148
Prugniel, Ph., Soubiran, C. 2001, A&A, 369, 1048
Prugniel, Ph., Soubiran, C. 2004, arXiv:astro-ph/0409214
Prugniel, Ph., Koleva, M., Ocvirk, P., Le Borgne, D., Soubiran, C. 2007a, in IAU Symp. 241, ed. A. Vazdekis, & R. F. Peletier, 68
Prugniel, Ph., Soubiran, C., Koleva, M., & Le Borgne, D. 2007b, arXiv:astro-ph/0703658
Riess, A. G. et al. 1998, AJ, 116, 1009
Riess, A. G. et al. 2009, ApJ, 699, 539
Roseboom, I. G. et al. 2006, MNRAS, 373, 349
Samushia, L. & Ratra, B. 2006, ApJ, 650, L5
Spergel, D. N. et al. 2007, ApJS, 170, 377
Stern, D., Jimenez, R., Verde, L., Kamionkowski, M., Standford, S. A. 2010, J. Cosmology Astropart.Phys, 02, 008
Simon, J., Verde, L., Jimenez, R. 2005, Phys. Rev. D, 71, 123001
Schawinkski, K. et al. 2007, ApJS, 173, 512
Wang, H., & Zhang, T.-J., 2012, ApJ, 748, 111
Wang, Y., & Tegmark, M. 2004, Phys. Rev. Lett., 92, 241302
Wei, H. 2010, Phys. Lett. B, 687, 286
Worthey, G., Faber, S. M., González, J. J., Burstein, D. 1994, ApJS, 94, 687
Wu, Y., Singh, H. P., Prugniel, Ph., Gupta, R., Koleva, M. 2011a, A&A, 525, A71
Wu, Y. et al. 2011b, RAA, submitted
Xu, L. X. 2012, Phys. Rev. D, 85, 123505
Yang, X.-J., & Chen, D.-M. 2009, MNRAS, 394, 1449
Yi, Z. L.,& Zhang, T.-J. 2007, Mod. Phys. Lett. A, 22, 41
Zhang, T.-J., Ma, C., & Lan, T. 2010, Adv. Astron., article id. 184284
Zhang, J. F., Zhang, X. & Liu, H. Y. 2007, EPJC, 52, 693
Zhang, H. S., & Zhu, Z. H. 2008, J. Cosmology Astropart.Phys, 03, 007